Mesh Sensitivity Analysis of an Entrained Flow Biomass Gasifier: A CPFD Study

Ramesh Timsina[a,] *, Zahir Barahmand[a]

[a] *Department of Process, Energy and Environmental Technology, University of South-Eastern Norway, Porsgrunn*
ramesh.timsina@usn.no

Abstract

Biomass such as agricultural waste, forestry waste, municipal solid waste, and industrial waste, are renewable energy sources that may be used to produce biofuels. Biomass gasification is an effective and promising technology for converting any biomass into valuable products that can contribute considerably to renewable energy generation. In the manufacturing industry, computer-based simulations, improving production processes while incorporating sustainable industrial strategies, are rising. In the Computational Fluid Dynamics (CFD) scientific community, the reliability of computational prediction of findings is a rising problem. Mesh independence is crucial since it may determine if the solution obtained is independent of the mesh resolution. In CFD models, there are a variety of strategies for discovering a mesh independence test such as the grid resolution, general Richardson extrapolation, and Grid Convergence Index (GCI). In the grid resolution technique, the mesh size gradually increases until no meaningful performance improvement can be seen due to the larger mesh size. The present study aims to analyze the mesh independence test using the grid resolution method on an entrained flow biomass gasifier and investigate the model's sensitivity to parameters such as reactants' inlet temperature, product gas compositions and flow rate. To achieve this goal, four different scenarios were defined employing a series of Computational Particle Fluid Dynamics (CPFD) simulations using Barracuda® v21.0.1. The results confirmed that within the range of 25000 and 200000 cells, synthesis gas production decreased by almost 2 percent, which is not significant.

Keywords: mesh sensitivity analysis, mesh independence test, CPFD, gasification, entrained flow gasifier

1 Introduction

As the fourth-largest source of energy after coal, petroleum, and natural gas, biomass contributes a significant percentage of global primary energy consumption (Shah and Venkatramanan, 2019). Biomass now accounts for around 15% of total global energy use in all forms (Ankolekar and Kulkarni, 2018).

Biofuels, such as agricultural, forestry, municipal solid waste, and industrial waste, are renewable energy sources that may be used to produce solid or liquid fuels. Gasification, pyrolysis, and direct combustion are the main thermochemical conversion technologies (Pereira *et al.*, 2012), where gasification is the most efficient process (Purohit, 2009). Gasification is the partial oxidation of biomass (carbonaceous materials) at elevated temperatures to generate synthesis gas (commonly known as syngas), primarily carbon monoxide and hydrogen (Zamarripa *et al.*, 2013). The product gas from the gasification process consists of CH_4, CO, CO_2, and H_2, as well as other light gases such as ethane (C_2H_6) and propane (C_3H_8) in addition to various condensable gases. Moreover, this process produces some amounts of biochar, tars, and ashes (Pereira *et al.*, 2012). Biomass gasification is an effective and promising technology for converting any biomass into valuable products by thermochemical conversion, which contributes considerably to renewable energy generation.

There are various developments and studies of numerical simulation tools, such as Computational Fluid Dynamics, with high prediction accuracy within a reasonable simulation time to predict such complex flows. Due to the presence of three-phase in the systems, entrained flow reactors are the most challenging and most complex systems in multiphase modelling. The CFD scientific community is becoming increasingly concerned with the accuracy of computational outcomes prediction. Therefore, several important concerns arise (Seeni *et al.*, 2021): Are computational results reliable? How can the accuracy or validity of CFD predictions be evaluated? These questions are posed because of the uncertainty associated with CFD-generated data. As a result, procedures for verification and validation have been created to address this developing issue. Code and solution verification are both components of verification. Analytical, very precise hybrid analytical-numerical, and manufactured solutions to mathematical models can be used for verification. Validation often entails determining the accuracy of a mathematical model's representation of the

physical processes of interest using carefully designed and conducted experimental data (Baliga and Lokhmanets, 2016).

A mesh independence study (or so-called mesh sensitivity) determines whether or not simulation results are independent of the underlying mesh (McDavid, 2001). There are several methods for determining a mesh independence test in CFD issues. The grid resolution, the general Richardson extrapolation, and the Grid Convergence Index (GCI) are three often utilized methods (Seeni et al., 2021). Grid Convergence Index - GCI is a technique for estimating discretization error even when subsequent mesh refinements are not integer multiples (Castedo *et al.*, 2019). Richardson's extrapolation is a numerical analysis approach for predicting the error in the answer by solving the issue with two alternative grid sizes, assuming the solution's functional form is known (Rao, 2001). In the grid resolution technique, the mesh size gradually increases until the performance improvement cannot be noticed due to the increased mesh size.

The current study aims to conduct a mesh sensitivity analysis using the grid resolution method on an entrained flow biomass gasifier and investigate the model's sensitivity for different parameters such as molar concentrations, flow rate, and temperature.

The paper is organized as follows: Chapter 2 provides a brief background, and Chapter 3 provides a mathematical description of the CPFD model. Chapter 4 details the developed computational model for the selected gasifier and simulation setup. The study's outcome is described in Chapter 5, and the conclusion is drawn at last.

2 Background

There are different CFD models available in the literature to study an entrained flow biomass gasification reactor at different levels of accuracy and depth (Fletcher et al., 1998, 2000; X. Gao et al., 2018; X. Y. Gao et al., 2014; Ku et al., 2014; Slezak et al., 2010). Most models account for the chemical and physical properties inside the gasifier, commonly known as the non-equilibrium/kinetic model. The models are generally validated using data from a certain gasifier. This can create a certain room for uncertainty as the operation of commercial gasifiers could vary significantly. Variations in various aspects include air-blown, oxygen-blown, non-pressurized, pressurized, single-stage, multiple-stage, dry feed, slurry feed, swirling flow, non-swirling flows, refractory insulations, etc. are the common example. The current study aims to develop a CPFD model considering these different aspects to simulate an entrained flow biomass gasification reactor within a reasonable time frame with certain efforts and accuracy. Fig. 1 shows the relationship between time, effort, and accuracy for any computational model.

Figure 1: Inter-relation between time, efforts, and accuracy for CFD models.

The higher the time and effort invested while developing a CFD model, the higher the model's accuracy and vice versa. Therefore, a compromise must be made between efforts to build the model, accuracy of calculations, and calculation time (Kaczor *et al.*, 2020). In addition to this, model validation is an important aspect of their applications. A validated CFD model becomes a credible engineering tool for further applications.

3 Mathematical modelling equations

The continuity gives the gas-phase mass and momentum conservation equations, and the Navier-Stokes equations are represented by Eq. (1) and (2), respectively.

$$\frac{\partial(\alpha_g \rho_g)}{\partial t} + \nabla \cdot (\alpha_g \rho_g \vec{u}_g) = \delta \dot{m}_p \quad (1)$$

$$\frac{\partial}{\partial t}(\alpha_g \rho_g \vec{u}_g) + \nabla \cdot (\alpha_g \rho_g \vec{u}_g \vec{u}_g) = -\nabla p + F + \alpha_g \rho_g g + \nabla \cdot (\alpha_g \tau_g) \quad (2)$$

where α, ρ and $\vec{u}$ represent the volume fraction, density, and velocity vector, respectively. $\delta \dot{m}_p$ is the gas mass production rate per volume formed from the particle-gas chemical reaction. In the case of the cold flow model with no chemical reaction, $\delta \dot{m}_p$ becomes zero. P is the mean flow gas pressure, g is the acceleration due to gravity, τ_g is the fluid phase stress tensor, and F is the inter-phase momentum transfer rate per unit volume (particle to fluid phase). For a Newtonian fluid, the gas phase stress tensor for each species, τ_g is given by:

$$\tau_{g,ij} = \mu \left[\left(\frac{\partial u_i}{\partial x_j} + \frac{\partial u_j}{\partial x_i} \right) - \frac{2}{3} \mu \delta_{ij} \frac{\partial u_k}{\partial x_k} \right] \quad (3)$$

where μ is the shear viscosity, which is the sum of the laminar shear viscosity and the turbulence viscosity defined in the Smagorinsky turbulence model (Smagorinsky, 1963), the model is given in equation 4 (Snider *et al.*, 2011).

$$\mu_t = C_s \rho_g \Delta^2 \left(\frac{\partial u_i}{\partial x_j} + \frac{\partial u_j}{\partial x_i} \right) \quad (4)$$

The Smagorinsky coefficient C_s has a default value of 0.01. Δ is the subgrid length and is given by:

$$\Delta = (\delta x \delta y \delta z)^{1/3} \quad (5)$$

The interphase momentum transfer (F) in Equation 2 is given by:

$$F = \iiint f \left[m_p \left\{ D_P(\vec{u}_g - \vec{u}_p) - \frac{\nabla P}{\rho_p} \right\} + \vec{u}_p \frac{dm_p}{dt} \right] dm_p d\vec{u}_p dT_p \quad (6)$$

In terms of f, the fluid mass source in Eq. (1) is:

$$\dot{m}_p = - \iiint f \frac{dm_p}{dt} dm_p d\vec{u}_p dT_p \quad (7)$$

where the time-rate-of-change of particle mass dm_p/dt is the rate of change of the particle mass produced by chemical processes. The particle acceleration can be calculated by:

$$\frac{du_p}{dt} = D_p(\vec{u}_g - \vec{u}_p) \frac{\nabla P}{\rho_p} - \frac{\nabla \tau_p}{\alpha_p \rho_p} + g + \frac{u_p' - \vec{u}_p}{\tau_D} \quad (8)$$

where ρ_p is the particle mass density, τ_p which can be derived by Eq. (9) is the solids contact stress, which depends on spatial location, D_p is the drag function, which depends on the particle size, velocity, position, and time. u_p' is the local mass-averaged particle velocity. τ_D is a particle collision damping time (O'Rourke and Snider, 2010).

$$\tau_p = \frac{P_s \alpha_p{}^{\beta}}{max[(\alpha_{cp} - \alpha_p),\ \varepsilon(1 - \alpha_p)]} \quad (1)$$

Particle normal stress is exerted on a solid until the solid reaches the particle-mean velocity (Snider et al., 2011). P_s is a constant (Pa), α_{cp} is the particle volume fraction at close packing, β is a constant (between 2 – 5) and ε is a very small number in the order of 10^{-8}. The solids volume fraction is related to the PDF f by:

$$\alpha_p = \iiint f \frac{m_p}{\rho_p} dm_p d\vec{u}_p dT_p \quad (2)$$

4 Simulation setup

The reactor dimensions as well as the reaction kinetics were adopted from the author's previous studies (Timsina *et al.*, 2021; Timsina *et al.*, 2020). As shown in Fig. 2, the reactor has 0.52 m in diameter with a conical outlet and 1.67 m in height. The biomass and the fluidizing agent were modelled as injection boundaries at the top, and a pressure boundary was defined at the bottom for product outflow from the reactor. The details of the injection boundary can be found in the author's previous study. Barracuda® v21.0.1 was the CFD software used for the simulations (Software©, 2022).

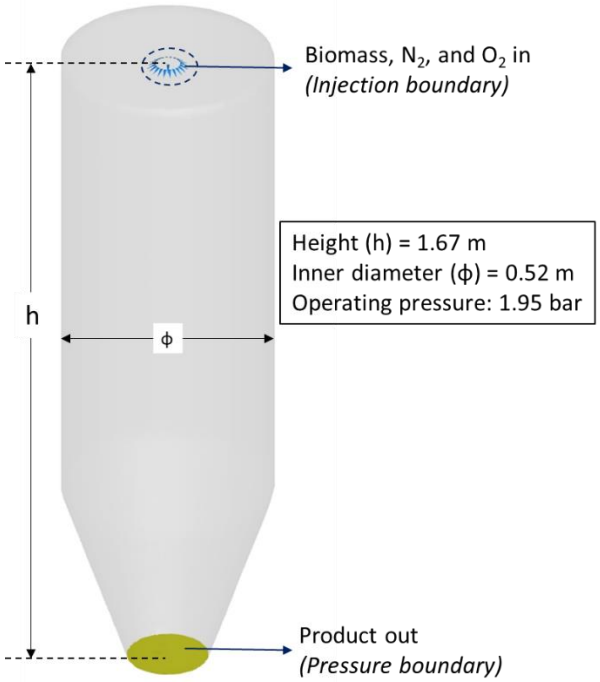

Figure 2: Boundary conditions

The Wen-Yu drag model was chosen due to the dilute solid phase where the gas volume fraction is higher than 0.8 (Cho *et al.*, 2020; Jayarathna *et al.*, 2019; Patel *et al.*, 1993), and the chosen particle model parameters are presented in Tab. 1.

Table 1: Particle phase model parameter

Drag model	Wen-Yu
Closed pack volume fraction	0.2
Maximum momentum redirection from collision	40%
Tangent to wall momentum retention	0.85
Normal to wall momentum retention	0.15

An injection boundary was chosen for the introduction of biomass particles into the reactor as it does not need an assistance of a fluid stream. The blue triangles with spheres at the top represent the injection points. A total of 20 injection points along the circle and one in the middle were defined in the model (Timsina *et al.*, 2021).

The grid dimensions in x, y, and z directions for each mesh are given in Tab. 2. The normalized grid size was checked to ensure they lie below the warning line. The grid refinements at the wall were not performed for all the meshes to have uniformity in simulation conditions. The built-in grid generator was used in Barracuda to generate the grid, and the

cells having a volume fraction less than 0.04 and aspect ratio higher than 5:1 were neglected. As a result, the Cartesian mesh of 25000 (25k), 50000 (50k), 100000 (100k), and 200000 (200k) cells gave the corresponding number of cells in Tab. 2.

Table 2: cell dimensions

No. of cells	ΔX	ΔY	ΔZ	Case
22743	19	19	63	1
48080	24	24	80	2
97061	31	31	101	3
193167	39	39	127	4

Four different meshes with 22743, 48080, 97061, and 193167 cells were tested, and the cross-sectional views are illustrated in Fig. 3. From here onwards, the four cases will be mentioned as 25k cells, 50k cells, 100k cells, and 200k cells for case numbers 1, 2, 3, and 4, respectively.

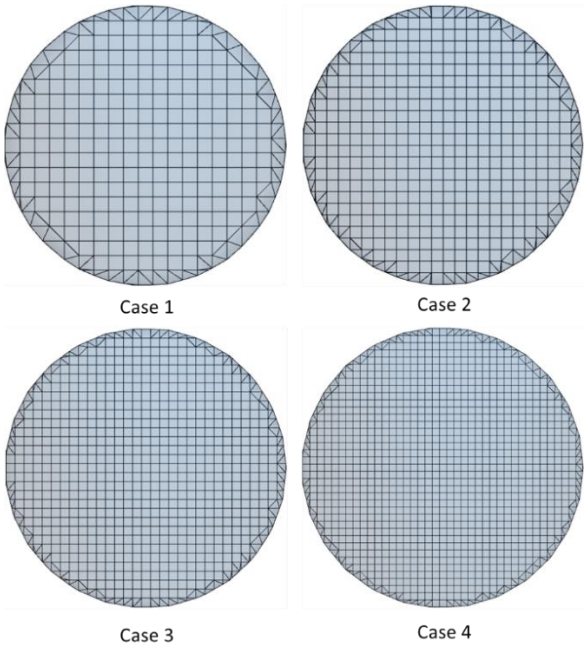

Figure 3: Cross-sectional view of different grids (top view)

5 Results and Discussions

Simulations were performed for four different grids with 25k, 50k, 100k, and 200k cells. In the grid resolution technique, the mesh size gradually increases until no meaningful performance improvement can be seen due to the larger mesh size. The computation is a three-dimensional non-isothermal with homogeneous and heterogeneous gasification chemistry. Simulations were carried out for 300 seconds of simulation time with a number density of 125000, and the gas composition, temperature, residence time, and flow rates were monitored. Average gas compositions were taken from the final 150 seconds of simulations. The bottom plane of the reactor gives the product gas from the reactor.

It is important to monitor the different grids' fluid temperature along the reactor. Fig. 4 shows the average fluid temperature along the gasifier. The temperature value was radially averaged at t =150s. The figure shows the highest fluid temperature at the reactor injection burner, suggesting that some degree of combustion prevails around this region of the gasifier. This is beneficial as it supplies the generated heat to the devolatilization of the biomass. The average fluid temperature in this region for 25k and 50k cells seems to fluctuate more than the 100k and 200k cells. This gives some stability to the reactor temperature profile in the burner region of the gasifier. The average temperature is almost the same for all the cases as we move downwards along the gasifier.

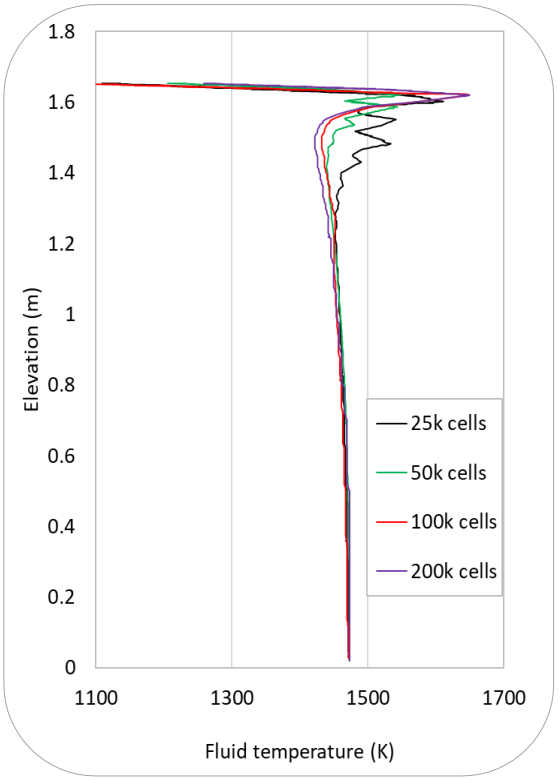

Figure 4: fluid temperature versus elevation. The fluid temperature is radially averaged.

As the thermal and chemical behavior are coupled together in such systems, a change in one parameter affects the changes in the other ones. Heat is supplied from reactor walls, and the gas is fed into a biomass gasifier. Chemical transformation, such as breaking chemical bonds, gives sensible heat, which changes the temperature. Therefore, product gas composition and flow rates were monitored for all the cases during the simulations. Fig. 5 shows the product gas flow rate from the outlet boundary of the reactor. After the reactor reached the steady state, which took around 50 seconds, the mass flow rate of

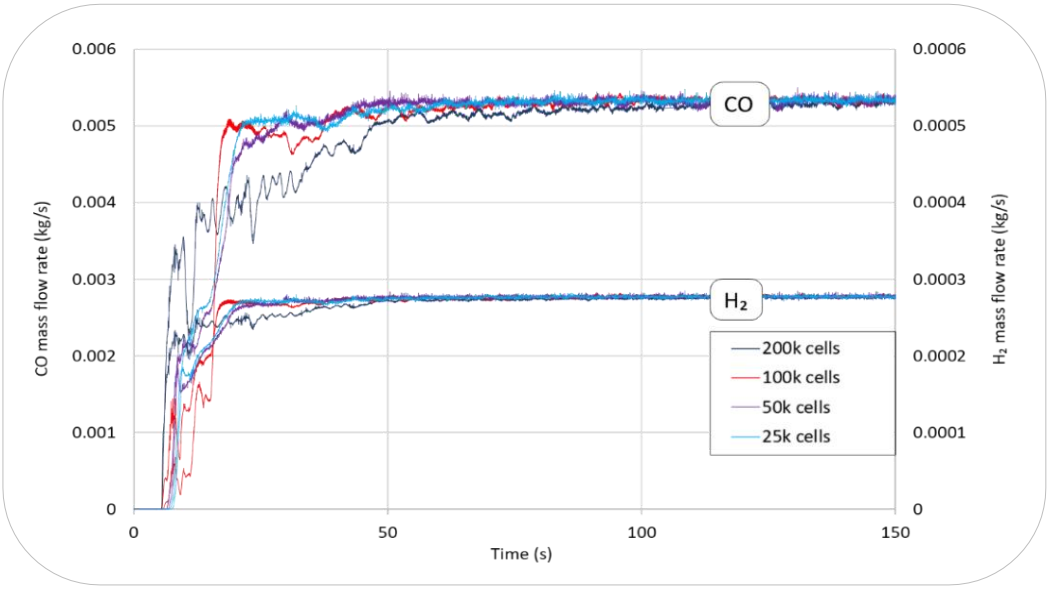

Figure 5: carbon monoxide and hydrogen mass flow rate at the outlet boundary

CO and H_2 stabilized around their median value. Production of gases starts after around 5 seconds of simulation. There was a high fraction of the CO_2 at the start representing the combustion process; however, after the steady-state, the average composition for all the gas species varied around their mean value. To look closely, only CO and H_2 are taken to compare the four different grids. A certain level of variation at steady in the gas production illustrates different physical and chemical transformations occurring inside the reactor. To compare the different cases, the average molar composition of major gas species (CO, H_2, and CH_4) is compared in Tab. 3.

Table 3: average molar concentrations

Case	Average molar concentration			% Variation wrt 25k cells		
	CO	H_2	CH_4	CO	H_2	CH_4
1	0.20	0.01	0.01	-	-	-
2	0.20	0.01	0.01	-0.32	0.16	-0.92
3	0.20	0.01	0.01	-0.52	0.08	-0.92
4	0.20	0.01	0.01	-1.72	-0.22	-2.09

As the data show that there is little variation between the four different cases. The absolute percentage variation of the molar composition of CO, H_2, and CH_4 varies from 0.32% to 2.1%. This shows a minor and not significant variation, and there should be a trade-off between the number of cells and the simulation timing.

Looking only at the reactor hydrodynamics can be tricky when doing resolution studies because the number of pixels drawn in Tecplot (an output result viewer for Barracuda) corresponds to the number of clouds in the simulation. This makes the high-resolution cases look much denser even if they have the same volume fraction and mass of particles. This limitation of the Tecplot leads us to present the simulation timing for the considered cases. The simulation time increased exponentially with the increase in the number of cells in the system. The simulation time in hours (t) varied according to the $t = 24.185e^{0.00002n}$, where n represents the total number of cells (25000, 50000, 100000 & 200000). In numbers, the corresponding simulation time were 29, 78, 230 and 1100 hrs respectively for the case 1, 2, 3, and 4 respectively. In order to visualize the simulation timing in terms of simulation results, CFL is monitored for all the cases. The timestep for any transient CFD model is an important parameter. The time step must be small enough to represent any rapidly changing variables of interest. If the time step is too big, an accumulation of errors will occur (Zhang *et al.*, 2000). To resolve this problem, a varying time step can be utilized with the help of the Courant-Friedrichs-Lewy (CFL) number, as shown in Eq. (11):

$$CFL = \frac{v\,\Delta t}{\Delta x} \qquad (3)$$

where v is velocity, Δt is time step and Δx is cell size. Fig. 6 shows the CFL for all the cases.

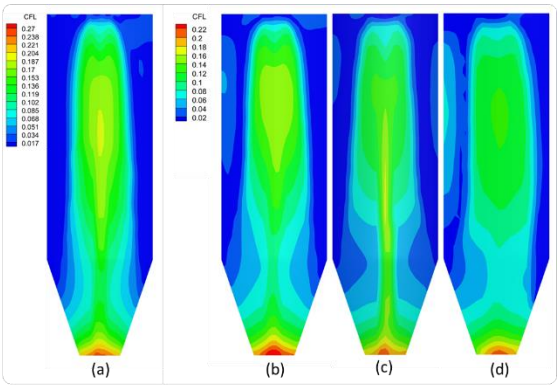

Figure 6: CFL for cases with (a) 200k, (b) 100k, (c) 50k and (d) 25k cells

With an increase in cell size, CFL seems to increase linearly. However, the velocity of the particle plays an important role. As shown in the figure, CFL decreased with an increase in the number of cells. CFL is comparatively lower for case number four compared to other cases. The higher the number of cells, the more continuous the CFL profile inside the reactor. Courant–Friedrichs–Lewy number gives the amount of information traveling across a computational cell in a unit of time. CFL number higher than one gives an inaccurate solution and could potentially lead to divergence of the results. The timestep is an important aspect during a CFD simulation and should be selected carefully such that all the physics of interested parameters are resolved in that time step. The additional cells are allowing the model to capture more details of the flow profile. However, the 100k-cell resolution looks similar to that of 200k-cell resolution, so that the 100k-cell case could be sufficient in terms of cell resolution.

6 Conclusions

A CPFD model was developed in Barracuda® v21.0.1 using the MP-PIC modelling approach. The model was used to simulate a biomass gasification process in an entrained flow gasifier. To conduct a mesh sensitivity analysis through a mesh resolution technique, the model was simulated with four different numbers of cells (from 25k to 200k) to see the effect of grid resolution in terms of molar concentrations, flow rate, and temperature along the gasifier. Although there was a considerable difference in hydrodynamics inside the reactor in different cases, the results show minor variations (maximum 2 percent) in main output variables such as reactor temperature, gaseous product flow rate, and composition. Therefore, it can be concluded that the system was not sensitive to the number of cells within the selected mesh sizes. For further studies, it is suggested to perform this sensitivity analysis with higher resolutions (over millions); however, it will be costly.

Acknowledgment

The authors would like to thank the University of South-Eastern Norway (USN) for providing the necessary software for the simulation works.

References

Ankolekar, V., and Kulkarni, S. (2018). Briquetting of agricultural biomass: an overview. *International Journal for Research in Applied Science and Engineering*, *6*(2), 1681-1685.

Baliga, B. R. R., and Lokhmanets, I. Y. (2016). Generalized Richardson extrapolation procedures for estimating grid-independent numerical solutions. *International Journal of Numerical Methods for Heat & Fluid Flow*.

Castedo, R., Reifarth, C., Santos, A. P., Losada, J. J., López, L. M., Chiquito, M., and Mancilla, J. M. (2019). Application of grid convergence index to shock wave validated with LS-DYNA and ProsAir. *Ingeniería e Investigación*, *39*(3), 20-26. doi:10.15446/ing.investig.v39n3.81380

Cho, S., Park, C., Lee, J., Lyu, B., and Moon, I. (2020). Finding the best operating condition in a novel process for explosive waste incineration using fluidized bed reactors. *Computers & Chemical Engineering*, 107054. doi:10.1016/j.compchemeng.2020.107054

Jayarathna, C. K., Balfe, M., Moldestad, B. M., and Tokheim, L.-A. (2019). Improved multi-stage cross-flow fluidized bed classifier. *Powder Technology*, *342*, 621-629. doi:10.1016/j.powtec.2018.10.026

Kaczor, Z., Buliński, Z., and Werle, S. (2020). Modelling approaches to waste biomass pyrolysis: a review. *Renewable Energy*, *159*, 427-443.

McDavid, R. M. (2001). Macroscopic Modeling. In K. H. J. Buschow, R. W. Cahn, M. C. Flemings, B. Ilschner, E. J. Kramer, S. Mahajan, & P. Veyssière (Eds.), *Encyclopedia of Materials: Science and Technology* (pp. 4720-4732). Oxford: Elsevier.

Patel, M., Pericleous, K., and Cross, M. (1993). Numerical modelling of circulating fluidized beds. *International Journal of Computational Fluid Dynamics*, *1*(2), 161-176. doi:10.1080/10618569308904470

Pereira, E. G., Da Silva, J. N., de Oliveira, J. L., and Machado, C. S. (2012). Sustainable energy: a review of gasification technologies. *Renewable and sustainable energy reviews*, *16*(7), 4753-4762.

Purohit, P. (2009). Economic potential of biomass gasification projects under clean development mechanism in India. *Journal of Cleaner Production*, *17*(2), 181-193.

Rao, S. S. (2001). FINITE ELEMENT METHODS. In S. Braun (Ed.), *Encyclopedia of Vibration* (pp. 530-544). Oxford: Elsevier.

Seeni, A., Rajendran, P., and Mamat, H. (2021). A CFD Mesh Independent Solution Technique for Low Reynolds Number Propeller. *CFD Letters*, *11*(10), 15-30. Retrieved from https://www.akademiabaru.com/submit/index.php/cfdl/article/view/3187

Shah, S., and Venkatramanan, V. (2019). Advances in microbial technology for upscaling sustainable biofuel production. In *New and future developments in microbial biotechnology and bioengineering* (pp. 69-76): Elsevier.

Smagorinsky, J. (1963). General circulation experiments with the primitive equations: I. The basic experiment. *Monthly weather review*, *91*(3), 99-164. doi:10.1175/1520-0493(1963)091<0099:GCEWTP>2.3.CO;2

Snider, D. M., Clark, S. M., and O'Rourke, P. J. (2011). Eulerian–Lagrangian method for three-dimensional thermal reacting flow with application to coal gasifiers. *Chemical engineering science*, *66*(6), 1285-1295. doi:10.1016/j.ces.2010.12.042

Software©, C. (2022). CPFD Software. Retrieved from https://cpfd-software.com/

Timsina, R., Thapa, R. K., Moldestad, B. M., and Eikeland, M. S. (2021). Computational particle fluid dynamics simulation of biomass gasification in an entrained flow gasifier. *Chemical Engineering Science: X, 12*, 100112.

Timsina, R., Thapa, R. K., Moldestad, B. M. E., and Eikeland, M. S. (2020). *Simulation of entrained flow gasification reactor with Multi Phase Particle in Cell (MP-PIC) approach.* Paper presented at the 61st SIMS Conference on Simulation and Modelling SIMS 2020, Online.

Zamarripa, M., Hjaila, K., Silvente, J., and Espuña, A. (2013). Simplified model for integrated Supply Chains Planning. In *Computer Aided Chemical Engineering* (Vol. 32, pp. 547-552): Elsevier.

Zhang, G.-Q., Ernst, L. J., and de Saint Leger, O. (2000). *Benefiting from thermal and mechanical simulation in micro-electronics* (1st ed.). Netherlands: Springer.